Regular Article

PHYSICAL CHEMISTRY RESEARCH
Published by the
Iranian Chemical Society
www.physchemres.org
info@physchemres.org

Phys. Chem. Res., Vol. 12, No. 4, 1037-1047, December 2024
DOI: 10.22036/pcr.2024.451396.2511

Synthesis and Characterization of Porous SiO_2/C Composite from Rice Husks through Activation with Sodium Hydroxide and its Application in Pouch Cell Li-Ion Batteries

Thanh Liem Pham[a,c], Thien Trung Nguyen[b,c], Tran Bich Tram Vo[a,c], Tan Phat Vu[a,c], Van Man Tran[a,c] and My Loan Phung Le[a,c,*]

[a]*Applied Physical Chemistry Laboratory, University of Science, Ho Chi Minh City 70000, Vietnam*
[b]*Central Laboratory for Analysis, University of Science, Ho Chi Minh City 70000, Vietnam*
[c]*Vietnam National University Ho Chi Minh City 70000, Vietnam*
(Received 6 April 2024, Accepted 12 August 2024)

SiO_2 is considered a promising candidate for future high-power energy Li-ion batteries thanks to its affordability and accessibility, low discharge potential (0.7 V *vs*. Li^+/Li), and high specific capacity of 1965 mAh g^{-1}. Rice husk naturally contains SiO_2 in the form of nanoparticles, making it a reasonably priced anode material with a high silica content. In this study, amorphous and porous SiO_2/C anode materials are successfully synthesized by calcinating rice husk with NaOH, an activating agent. The prepared anode materials exhibited a surface area of 210 m^2 g^{-1} with pore sizes ranging from 50 to 100 nm. In addition, SiO_2 particles were coated by a 3-5 nm carbon layer to depress volume expansion and thus enhance cycling performance. The SiO_2/C anode provided a capacity of 1625.3 mAh g^{-1} in the 1st cycle and maintained around 645 mAh g^{-1} in the following 50 cycles. The optimal negative/positive capacity ratios were determined in coin cells and the high-capacity pouch cells (4 × 6 cm^2, 40 mAh) were further assembled to demonstrate a potential application of SiO_2/C in high-power Li-ion batteries.

Keywords: Rice husk, SiO_2/C anode, pouch cell, Li-ion batteries

INTRODUCTION

The rapid development of portable electronic devices, electric vehicles, and large-scale energy storage systems has resulted in an increasing demand for high-capacity lithium-ion batteries (LIBs) [1-3]. The graphite currently employed in commercial LIBs suffers from low capacity and low-rate capability, which severely restricts the development of LIBs. Consequently, it is crucial to develop a high-capacity anode to enhance the performance of high-energy density LIBs. Among many advanced anode materials, SiO_2 is becoming a promising candidate thanks to its high specific capacity of 1965 mAh g^{-1}, facile preparation process, low discharge potential (<0.7 V *vs*. Li^+/Li), affordability, and accessibility [2-5].

Nonetheless, the application of SiO_2 is still impeded by the extreme volume change and low electronic conductivity, leading to poor rate and limited cycling life [6-8]. Generally, nanostructure engineering and carbon material coating are effective methods to improve structural stability and electrical conductivity [9-11]. Therefore, surface morphology and micro/nano-structure engineering have been utilized to design mesoporous SiO_2 with a hollow structure. This design reduces the volume variation of SiO_2 and electrode pulverization during Li^+ intercalation/deintercalation [12]. Graphene, carbon nanotubes, and other carbon nanostructures enhance structural stability and high ion/electron transport of

*Corresponding author. E-mail: lmlphung@hcmus.edu.vn

mesoporous Si/SiO_2. However, it continues to substantially hinder the production of SiO_2 nanoparticles that exhibit uniform size, manageable microstructure, and shape [13]. Furthermore, the typical coating materials (graphene, carbon nanotubes, *etc*.) are either prohibitively expensive or difficult to mass produce [14-16]. Thus, it is highly desired to prepare SiO_2/C from low-cost renewable feedstocks.

Recently, numerous research has been dedicated to exploring the efficient utilization of biomass resources to produce electrode materials. This has proven critical in mitigating environmental waste pollution and curtailing production costs [17-22]. The annual production of rice husk ranges from 120 to 150 million tons worldwide, making it a readily available agricultural byproduct [23-24]. The material is economical, containing a high silica content (15-20 wt%), and the silica in rice husk is present naturally as nanoparticles [25-28]. Utilizing rice husk to synthesize composites with silica and carbon eliminates the need for additional carbon or silica sources and artificial dispersion of the materials. Recently, the research work of J. Lang *et al*. treated the surface of rice husk ash with ethanol, and sulfuric acid to remove impurities and synthesize a mesoporous and macroporous porous SiO_2@Carbon material by hydrothermal method for a battery capacity of about 2200 mAh g^{-1} at 0.2C [29]. M. Taufik group used silica gel extracted from rice husks and Mg powder to synthesize nano Si with a capacity of around 1750 mAh g^{-1} and remained above 1000 mAh g^{-1} after 200 cycles [30].

Carbon sources from biomass materials obtained by direct carbonization typically have a relatively low surface area and porosity, leading to locking Li^+ channels and hindering Li^+ diffusion during operation [31-33]. However, anode materials with a high surface area could increase internal resistance due to the formation of thick solid electrolyte interphase (SEI) layers, leading to low electrochemical performance. Therefore, it is essential to activate rice husk effectively in synthesis processes to improve the material's surface area and porosity and to enhance the benefits of its structural features and electrochemical properties. Among the activation agents for rice husk, alkali hydroxides, such as NaOH and KOH, are usually used to activate rice husk because of their excellent porosity [34-37]. In this study, SiO_2/C anode materials are derived from Vietnamese rice husks through the application of NaOH as an activating agent. This selection is predicated upon the supposition that the lower ionic radius of Na in relation to K may engender a diminution in the resultant products' surface area, thereby rendering them more amenable for deployment in Li-ion battery systems. The as-prepared materials have been matched with commercial $LiFePO_4$ (LFP) cathodes with suitable physicochemical properties at an optimal negative/positive capacity ratio (N/P ratio). These cells perform good electrochemical properties in coin-type full cells and pouch-type full cells at a capacity of 40 mAh.

EXPERIMENTAL

Synthesize of SiO_2/C Anode

A 1000 g rice husk (Long An province, Vietnam) was soaked into a solution of HCl (10 wt%, aqueous, Sigma Aldrich) for 12 h to remove impurities. Then, the materials were washed with distilled water until pH reached 7.0-7.5. The pretreated rice husk was dried at 80 °C for 12 h before crushing into small fragments (< 1 mm). The rice husk ash (RHA) was synthesized by calcinating pretreated rice husk in dry air (N_2/O_2 4:1) at 300 °C for 1 h. After that, the RHA and NaOH (97%, powder, Sigma Aldrich) were mixed at a mass ratio of 1:2; the mixture was calcinated at 800 °C in an Argon atmosphere for 1 h. Finally, the materials were washed with distilled water until pH reached 7.0-7.5 and dried at 80 °C for 12 h. The final products, SiO_2/C, were stored in the dehumidifying cabinet.

Electrode Fabrication Process

The anode slurry consists of 90 wt% SiO_2/C, 5 wt% carbon black (super P, MTI), and 5 wt% sodium carboxymethyl cellulose (Industrial grade, CMC, MTI) as a binder dissolved in deionized water. The mixture was prepared by a mixing machine (Thinky mixer, Japan) and then cast onto a Cu-foil. The anodes were roll-pressed at room temperature and punched into circles with a diameter of 14 mm for coin cell and 45 × 58 mm for pouch cell fabrication. Then, the electrodes were dried at 80 °C for 12 h in a vacuum oven. The anode thickness was controlled from 20 to 40 μm.

The cathode electrodes were fabricated by mixing $LiFePO_4$ (LFP, MTI), carbon black (super P, MTI), and

Table 1. The Composition of the Anode

Samples	SiO_2/C (wt %)	Graphite (wt %)	Carbon black (wt %)	CMC (wt %)
Graphite	-	90	5	5
SiO_2/C	90	-	5	5
SiO_2/C 5 wt%	5	85	5	5
SiO_2/C 10 wt%	10	80	5	5
SiO_2/C 20 wt%	20	70	5	5
SiO_2/C 50 wt%	50	40	5	5

poly(vinylidene fluoride) (99.5%, PVdF, MTI) dissolved in anhydrous N-methyl-2-pyrrolidone (99.5%, NMP, Merck) with a weight ratio of 80:15:5 onto an aluminum foil. The electrodes were roll-pressed at room temperature and punched into circles with a diameter of 12 mm for coin cell and 43 × 56 mm for pouch cell fabrication. Then, the electrodes were dried at 80 °C for 12 h in a vacuum oven. The cathode thickness was controlled from 40 to 60 μm.

Materials Characterizations

The morphology of SiO_2/C was characterized by Scanning electron microscopy (SEM, S-4800, Hitachi, Japan), and Transmission electron microscopy (TEM, JEM2010, JEOL, Japan). X-ray diffraction (XRD) patterns were collected on a D8 Advance Eco (Bruker, Germany) using Cu Kα radiation (λ = 1.5406 Å). N_2 adsorption/desorption experiments of the SiO_2/C material were performed *via* a Nova 3200e (Quantachrome, USA) at 77 K. The surface composition was evaluated by X-ray photoelectron spectroscopy (K-alpha, Thermo Scientific) using Al Kα (1486.6 eV).

Electrochemical Measurements

A solution of 1.0 M $LiPF_6$ in Ethylene carbonate:Diethyl carbonate:Dimethyl carbonate (1:1:1 vol.%) (99.9%, Solvionic, France) was used as an electrolyte. A 20 μm Trilayer Microporous Membrane (PP/PE/PP, Celgard 2320) was used as a separator. The cells were assembled in Argon filled glovebox. Cyclic voltammetry (CV) was used to determine the electrochemical kinetics of the SiO_2/C anodes at a scan rate of 0.1 mV s^{-1} with Li as counter electrode and reference electrodes, using an MPG2 potentiostat (Biologic, France). The cycling performance was evaluated using a Lanhe CT2001A (China). The coin-type half-cell SiO_2/C||Li cells were tested at the voltage range between 0.01 and 2.0 V at a current density of 100 mA g^{-1} in 50 cycles. The coin-type full-cell and pouch-type full cells were tested at the voltage range between 2.5 and 3.8 V at C/10 (1C = 150 mAh g^{-1}) in 50 cycles. The following formula calculates the negative electrode/positive electrode capacity ratio (N/P ratio):

$$\frac{N}{P} = \frac{Capacity_{anode}\,(mAh)}{Capacity_{cathode}\,(mAh)} = \frac{Specific\ capacity\left(\frac{mAh}{g}\right) \times Mass\ active\ (g)_{anode}}{Specific\ capacity\left(\frac{mAh}{g}\right) \times Mass\ active\ (g)_{cathode}} \quad (1)$$

RESULTS AND DISCUSSION

Figure 1a shows X-ray diffraction (XRD) patterns of rice husk ash (RHA) and SiO_2/C. A broad and weak diffraction peak with a center at 23° within the 2θ range of 15-30° indicates the presence of amorphous carbon and amorphous SiO_2. In addition, another peak at 43° is also ascribed to amorphous carbon [38-40]. Nitrogen adsorption-desorption measurements were used to determine the surface area and pore structure of SiO_2/C samples. As shown in Fig. 1b, the isotherms curve exhibited type IV according to the IUPAC classification, with a typical H4 type hysteresis loop, indicating that the SiO_2/C sample is both microporous and mesoporous. The surface area of SiO_2/C was calculated to be 210 $m^2\,g^{-1}$, which is relatively lower than other silica carbon materials using KOH or $ZnCl_2$ as activating agents. These results are compatible with an earlier report by the Watkinson group [41]. Moreover, SiO_2/C materials show a pore size

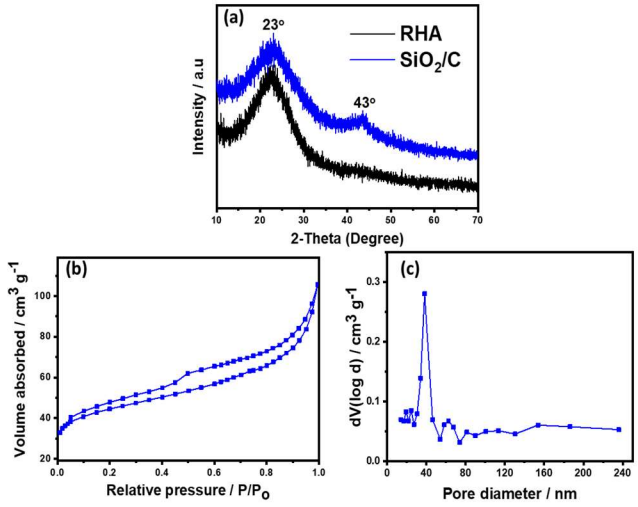

Fig. 1. (a) XRD patterns of RHA and SiO_2/C. (b) isotherm plot N_2 adsorption/desorption and (c) pore size distribution of SiO_2/C.

distribution from 1 to 60 nm, with a peak of 40 nm (Fig. 1c).

XPS analysis was further conducted to identify the chemical states of SiO_2/C samples. The XPS spectrum is shown in Fig. 2. In the C 1s spectra (Fig. 2a), there are three peaks at 284.6 eV, 285.7 eV, and 288.5 eV are attributed to the sp3 bonded carbon C-C, C-O, and C=O bonds, respectively [42]. As shown in Fig. 2b, the O 1s spectra between 527 and 540 eV displayed asymmetry and broadening that indicates the presence of several chemical states for oxygen in SiO_2/C. The first and second peaks at 531.6 and 533.4 eV correspond to Si-O-Si and Si-O bonds in SiO_2, respectively. In the SiO_2 structure, the bridging Si-O-Si bonds are more stable than single Si-O bonds. Therefore, the intensity of the former bonds is just over that of the latter. Because of the structural defects, a higher binding energy peak at 535.1 eV is observed in the O 1s spectra, similar to the peroxyl bridge Si–O–O–Si [43-45]. By contrast, there is only a peak of Si-O_4 (Si^{4+}) bonds at 104.6 eV, which confirms the existence of SiO_2 in SiO_2/C samples.

The morphology of RHA and SiO_2/C was evaluated using Scanning electron microscopy (SEM), Transmission electron microscopy (TEM), and Energy dispersive X-ray spectroscopy (EDS) techniques. The results are presented in Fig. 3, Fig. 4, and Fig. 5. The particle size of RHA ranges from 50-500 nm, as shown in Fig. 3a-b. In contrast, after calcination with NaOH as an activator, the surface of samples became porous, with pore sizes ranging from 50 to 100 nm. As suggested by EDS results (Fig. 4), Si content is 9.24 wt%, while C and O content are 64.88 wt% and 25.88 wt%, respectively.

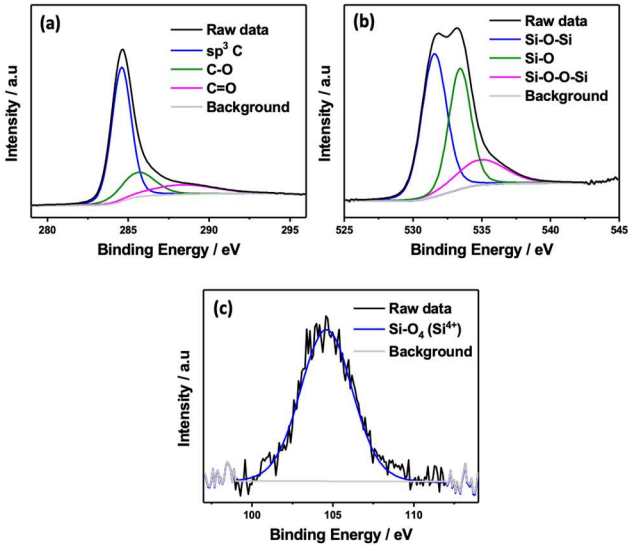

Fig. 2. XPS spectrum of SiO_2/C (a) C 1s, (b) O 1s, (c) Si 2p.

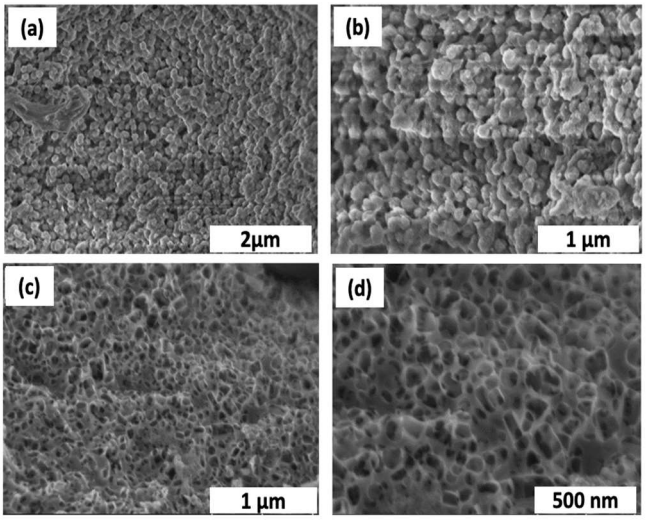

Fig. 3. SEM images of (a-b) RHA and (c-d) SiO_2/C.

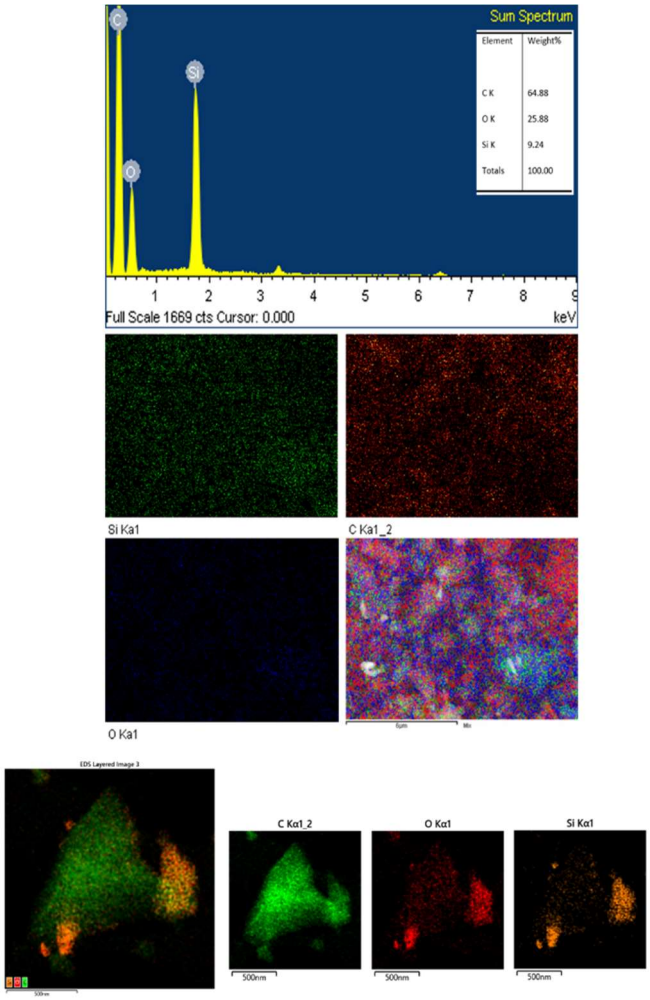

Fig. 4. EDS data of SiO_2/C materials.

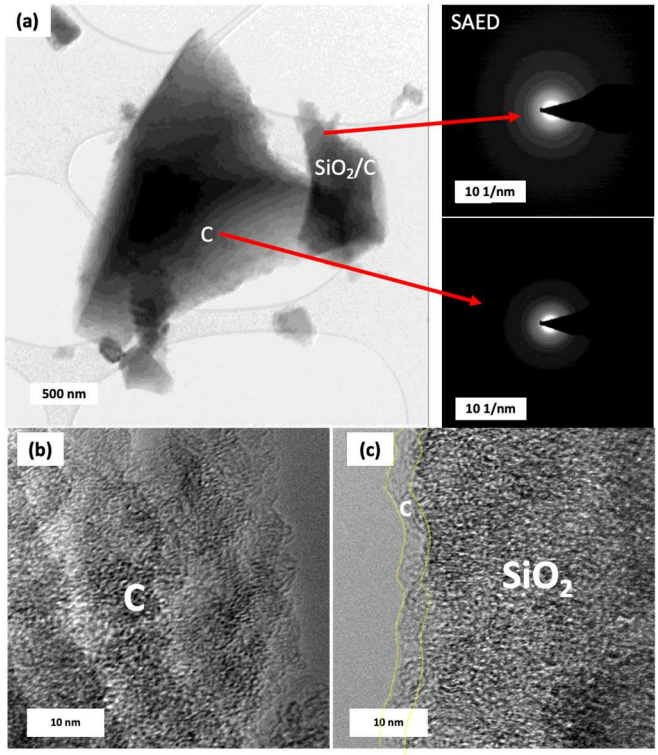

Fig. 5. TEM images and selected area electron diffraction (SEAD) patterns of SiO_2/C.

Figure 5a shows the selected area electron diffraction (SEAD) patterns of SiO_2/C. The diffused ring patterns are observed in both carbon and silica areas, indicating they are in the amorphous phase, which coincides with the XRD data (Fig. 1a). As shown in Fig. 5b-c, the SiO_2 materials are successfully coated by 3-5 nm carbon layer. Adding a carbon layer on SiO_2 nanoparticle surfaces not only enhances electron conductivity but also reduces the volume expansion of the anode materials during battery operation, thus improving battery performance.

The coin-type half-cell SiO_2/C||Li was examined by Cyclic voltammetry to evaluate the electrochemical kinetics of SiO_2/C anodes. In the first cycle, two broad reduction peaks were observed at 0.6 V and 1.3 V, while these peaks disappeared in the following cycles. The peak at 1.3 V is attributed to irreversible reactions between the electrolyte and anode electrode, forming Li_2O and Li_4SiO_4 compounds. These compounds are a protective layer to mitigate the stress build-up on SiO_2 particles due to volume expansion during the lithiation process. Moreover, the peak at 0.6 V is attributed to the formation of the SEI layers [46-48]. The cycling tests were performed from 0.01-2.0 V (*vs*. Li^+/Li) at 100 mA g^{-1}. As shown in Fig. 6b-c, the specific capacity underwent a significant drop (56.5%) in the 2nd cycle (706.5 mAh g^{-1}) compared to the 1st cycle (1625.3 mAh g^{-1}). It could be explained that the two irreversible reactions occurred in the first cycle to form protective and SEI layers. In the following cycles, the capacity remained stable at around 645 mAh $g^{-1,}$ with the Coulombic efficiency clustering around 99.3%. These findings align with a previous study conducted by the Wang group (~700 mAh g^{-1}) [49] or the Sun group (~ 800 mAh g^{-1}) [38]. The small differences might be from the precursors or electrolyte compositions.

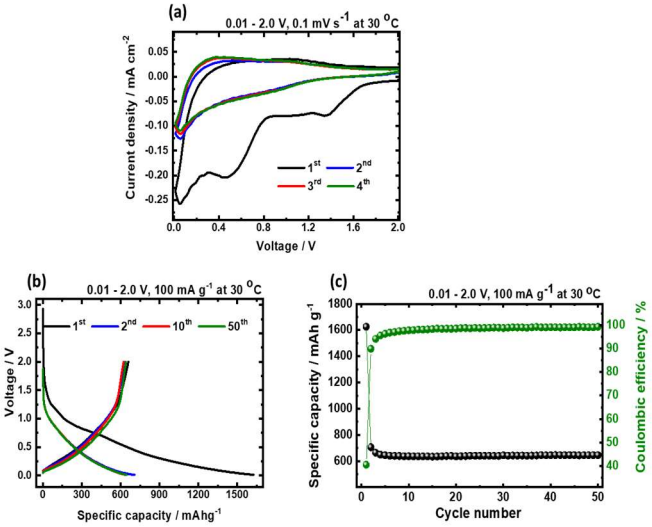

Fig. 6. (a) Cyclic voltammetry data, (b) Voltage profiles, and (c) Cycling performances of coin-type half-cell SiO_2/C || Li.

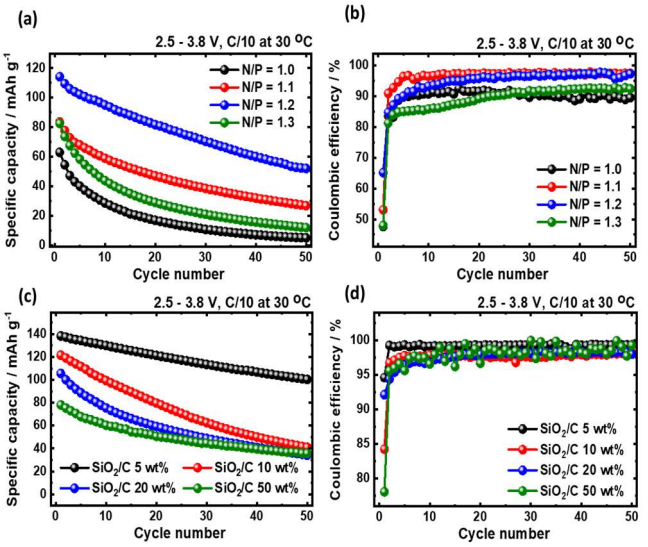

Fig. 7. Cycling performance of (a-b) coin-type full cell SiO_2/C|| LFP, (c-d) coin-type full cell graphite + SiO_2/C || LFP.

In full-cell design, the negative/positive electrode capacity ratio (N/P ratio) is an essential parameter to determine the battery's actual performance. At N/P ratio lower than 1.0, when the full cells are charging, the anode potential could close to 0 V (*vs.* Li^+/Li), increasing the lithium deposition potential and lithium plating, causing safety issues for the battery system. If the N/P ratio is too high, overcharging can occur in the cathode electrodes, leading to electrolyte as well as cathode materials oxidization [50-52]. Thus, SiO_2/C||LFP full cells with various N/P ratios of 1.0, 1.1, 1.2, and 1.3 were performed to determine the optimal N/P ratios. As shown in Fig. 7a, the cell with a N/P ratio of 1.2 exhibited the best cycling performance. The initial capacities of the N/P ratios 1.0, 1.1, 1.2, and 1.3 are 63.0, 83.6, 114.2 and 82.6 mAh g^{-1}, respectively. After 50 cycles, the capacity retention of the cell with an N/P ratio of 1.2 is 45.6%, and the figure for other cells averages around 10%. In addition, the Coulombic efficiency of N/P 1.1 and 1.2 samples is around 96%, as opposed to around 90% for the two other samples. These results are consistent with other reports for Li-ion batteries with LFP cathodes and graphite anodes from the Kumagai group [53].

SiO_2/C was mixed with commercial graphite with various weight percentages ranging from 5% to 50% to improve electrochemical properties further. These (graphite + SiO_2/C) || LFP coin-type full cells were assembled with a fixed N/P ratio of 1.2. The sample descriptions are shown in Table 1. The more SiO_2/C added, the lower the discharge capacity and capacity retention. Accordingly, the initial capacities of the SiO_2/C 5 wt%, SiO_2/C 10 wt%, SiO_2/C 20 wt%, and SiO_2/C 50 wt% anodes are 106.45, 130.6, 135.64, and 130.21 mAh g^{-1}, respectively. The cells employing the SiO_2/C 5 wt% anodes operated stably, while the cells employing other anodes showed a dramatic decrease in capacity during the cycling test. In detail, the cell using SiO_2/C 5 wt% anode exhibited the highest capacity at the 50th cycle with good capacity retention, typically 100.4 mAh g^{-1} and 72.6%. In contrast, the cell using SiO_2/C 50 wt% only exhibited 35.8 mAh g^{-1} and a capacity retention of 45.8%. Meanwhile, there is no considerable difference in Coulombic efficiency in these cells; the figure clusters around 98%. The excellent cycling performance of the SiO_2/C 5 wt% sample could be attributed to the role of SiO_2/C providing high capacity and graphite providing stable SEI layers, hindering volume expansion of SiO_2/C and high conductivity, thereby creating a synergistic effect that facilitates good electrochemical properties.

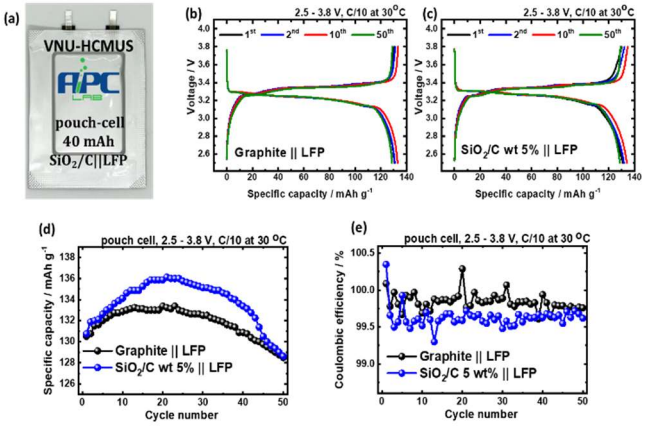

Fig. 8. (a) Photograph of pouch cell (4 × 6 cm^2, 40 mAh) (b-e) Voltage profile and cycling performance of pouch-type full cell with pure graphite anode and pouch cell with SiO_2/C 5 wt% anode.

Upscaling is essential to confirm the feasibility and practical usage of the R&D-developed components in a large battery format that closely fits industrial standards. Most research on electrolyte and anode/cathode materials for batteries is still limited to testing at the coin cell level. It makes it difficult to apply new findings to practical cells directly and neglects crucial aspects of SiO_2/C performance in real-world conditions [54]. Therefore, a single-layer pouch-type full cell (4 × 6 cm^2, 40 mAh) was fabricated to further demonstrate a high-capacity application of SiO_2/C anode. Fig. 8b-e compares voltage profiles and cycling performances of pouch-type full cells (N/P = 1.2) using SiO_2/C 5 wt% anode or pure graphite anode at current density of 0.1C. The initial capacity of these cells is around 138.5 mAh g^{-1}. However, the discharge capacity of the cell with SiO_2/C 5 wt% anode is much higher than that of the cell using pure graphite over the cycling test, and the discharge capacity is maintained at 98.5% after 50 cycles. These results further proved that the SiO_2/C materials will be potentially applied in large-scale LIBs.

CONCLUSIONS

The amorphous SiO_2/C materials were successfully synthesized from Vietnamese rice husk using NaOH as an activating agent. The sample's surface area is 210 m^2 g^{-1} with a pore size of around 40 nm. EDS and XPS data determine the existence and content of SiO_2 (~9.24 wt%). The SiO_2/C particles were successfully coated with a 3-5 nm carbon layer to suppress volume expansion during operation cycles. The SiO_2/C anode provided a capacity of 1625.3 mAh g^{-1} in the 1st cycle and maintained around 645 mAh g^{-1} in the following 50 cycles. The optimal N/P ratio for SiO_2/C||LFP full cells is 1.2, which delivered an initial capacity of 114.2 mAh g^{-1} with a capacity retention of 45.6% after 50 cycles. High mass loading pouch-type full cell (graphite + SiO_2/C 5 wt%) || LFP (4 × 6 cm^2, 40 mAh) performed good electrochemical properties, which showed initial capacity of 138.5 mAh g^{-1} with a capacity retention of 98.5% after 50 cycles. The research successfully confirmed the scalability, stability, suitability, and potential applications of SiO_2/C anodes derived from agricultural byproducts in the lithium-ion battery industry. The extensive utilization of these materials not only addresses the environmental challenge posed by agricultural by-products but also contributes to cost reduction in Li-ion battery production.

ACKNOWLEDGMENTS

This research is funded by the University of Science, VNU-HCM under grant number T2023-92.

REFERENCES

[1] Nzereogu, P.; Omah A.; Ezema, F.; Iwuoha, E.; Nwanya, A., Anode materials for lithium-ion batteries: A review. *Applied Surface Science Advances,* **2022**, *9*, 100233, https://doi.org/10.1016/j.apsadv.2022.100233

[2] Bi, J.; Du, Z.; Sun, J.; Liu, Y.; Wang, K.; Du, H.; Ai, W.; Huang, W., On the Road to the Frontiers of Lithium-Ion Batteries: A Review and Outlook of Graphene Anodes. *Adv. Mater.,* **2023**, *35*, 16, https://doi.org/10.1002/adma.202210734

[3] Liu, Y.; Shi, H.; Wu, Z. S., Recent status, key strategies and challenging perspectives of fast-charging graphite anodes for lithium-ion batteries. *Energy Environ. Sci.*, **2023**, *16*, 4834-4871, https://doi.org/10.1039/d3ee02213g.

[4] Loghavi, M. M.; Mohammdi-Manesh, H.; Eqra, R.; Ghasemi, A.; Babaiee, M., DFT Study of Adsorption of Lithium on Si, Ge-doped Divacancy Defected Graphene as Anode Material of Li-ion Battery. *Phys. Chem. Res.*, **2018**, *6*, 817-878, https://doi.org/10.22036/pcr.2018.148943.1543.

[5] Liu, H.; Sun, Q.; Zhang, H.; Cheng, J.; Li, Y.; Zeng, Z.; Zhang, S.; Xu, X.; Ji, F.; Li, D.; Lu, J.; Ci, L., The application road of silicon-based anode in lithium-ion batteries: From liquid electrolyte to solid-state electrolyte. *Energy Storage Mater*, **2023**, *55*, 244-263, https://doi.org/10.1016/j.ensm.2022.11.054.

[6] Phat, V.; Hoang, N.; Minh, D.; Trung, N.; Phung, L.; Man, T., Understanding the electrochemical properties of $Mn_7O_8SiO_4$ as promising anode material for low-cost batteries applications: Redox reaction and structural failure. *Mater. Lett.*, **2022**, *320*, 13223, https://doi.org/10.1016/j.matlet.2022.132231.

[7] Wang, C.; Gao, L.; Liu, M.; Xia, S.; Han, Y., Self-crystallization behavior of paraffin and the mechanism study of SiO_2 nanoparticles affecting paraffin crystallization. *Chem. Eng. J.*, **2023**, *452*, 139287, https://doi.org/10.1016/j.cej.2022.139287.

[8] Kong, F.; Zhou, W.; Peng, W.; Liang, C.; Wu, H.; Lin, N.; Wang, G.; Liu, D.; Feng, A.; Liu, X., Interface modified Si@SiO_2/PVDF composite dielectrics with synchronously ameliorative dielectric and mechanical properties. *J. Appl. Polym. Sci.*, **2023**, *140*, 31, https://doi.org/10.1002/app.54214.

[9] Ouyang, Q.; Li, G.; Zhang, X.; Zhao, X.; Wang, Y.; Wang, Q.; Fan, Z.; Wang, J.; Li, L., Towards high-capacity lithium-ion batteries: constructing hollow-structured SiO -based nanocube anode via a sequential coating strategy. *Chem. Eng. J.*, **2023**, *460*, 141762, https://doi.org/10.1016/j.cej.2023.141762.

[10] Ma, Z.; Zhu, J.; Zeng, F.; Yang, Z.; Ding, Y.; Tang, W., Structural Control and Optimization Schemes of Silicon-Based Anode Materials. *Energy Technol.*, **2023**, *11*, 6, https://doi.org/10.1002/ente.202201496.

[11] Li, Z.; Du, M.; Guo, X.; Zhang, D.; Wang, Q.; Sun, H.; Wang, B.; Wu, Y. A., Research progress of SiO-based anode materials for lithium-ion batteries. *Chem. Eng. J.*, **2023**, *473*, 145294, https://doi.org/10.1016/j.cej.2023.145294.

[12] Cheng, Z.; Jiang, H.; Zhang, X.; Cheng, F.; Wu, M.; Zhang, H., Fundamental Understanding and Facing Challenges in Structural Design of Porous Si-Based Anodes for Lithium-Ion Batteries. *Adv. Funct. Mater.*, **2023**, *33*, 26, https://doi.org/10.1002/adfm.202301109.

[13] Sharma, K.; Hooda, A.; Goyat, M.; Rai, R.; Mittal, A., A review on challenges, recent progress and applications of silica nanoparticles based superhydrophobic coatings. *Ceram. Int.*, **2022**, *48*, 5922-5938, https://doi.org/10.1016/j.ceramint.2021.11.239.

[14] Baig, N.; Kammakakam, I.; Falath, W., Nanomaterials: a review of synthesis methods, properties, recent progress, and challenges. *Mater. Adv.,* **2021**, *2*, 1821-1871, https://doi.org/10.1039/d0ma00807a.

[15] Slepičková, K. N.; Slepička, P.; Švorčík, V., Carbon Nanostructures, Nanolayers, and Their Composites. *Nanomaterials*, **2021**, *11*, 2368, https://doi.org/10.3390/nano11092368.

[16] Chauhan, D. S.; Quraishi, M.; Ansari, K.; Saleh, T. A., Graphene and graphene oxide as new class of materials for corrosion control and protection: Present status and future scenario. *Prog. Org. Coat.*, **2020**, *147*, 105741, https://doi.org/10.1016/j.porgcoat.2020.105741.

[17] Escobar, B.; Martínez-Casillas, D.; Pérez-Salcedo, K.; Rosas, D.; Morales, L.; Liao, S.; Huang, L.; Shi, X., Research progress on biomass-derived carbon electrode materials for electrochemical energy storage and conversion technologies. *Int. J. Hydrogen Energy*, **2021**, *46*, 26053-26073, https://doi.org/10.1016/j.ijhydene.2021.02.017.

[18] Liedel, C., Sustainable Battery Materials from Biomass. *ChemSusChem*, **2020**, *13*, 2110-2141, https://doi.org/10.1002/cssc.201903577.

[19] Manasa, P.; Sambasivam, S.; Ran, F., Recent progress on biomass waste derived activated carbon electrode materials for supercapacitors applications-A review. *J. Energy Storage*, **2022**, *54*, 105290, https://doi.org/10.1016/j.est.2022.105290.

[20] Zhang, M.; Zhang, J.; Ran, S.; Sun, W.; Zhu, Z., Biomass-Derived sustainable carbon materials in

energy conversion and storage applications: Status and opportunities. A mini review. *Electrochem. Commun.*, **2022**, *138*, 107283, https://doi.org/10.1016/j.elecom.2022.107283.

[21] Moradi, B.; Botte, G. G., Recycling of graphite anodes for the next generation of lithium ion batteries. *J. Appl. Electrochem.*, **2016**, *46*, 123-148, https://doi.org/10.1007/s10800-015-0914-0.

[22] Kumar, A.; Bhattacharya, T.; Mozammil, H. S.; Kumar N. A.; Hasnain M. S., Applications of biomass-derived materials for energy production, conversion, and storage. *Mater. Sci. Energy Technol.*, **2020**, *3*, 905-920, https://doi.org/10.1016/j.mset.2020.10.012.

[23] Shukla, S. S.; Chava, R.; Appari, S. A. B.; Kuncharam, B. V. R., Sustainable use of rice husk for the cleaner production of value-added products. *J. Environ. Chem. Eng.*, **2022**, *10*, 106899, https://doi.org/10.1016/j.jece.2021.106899.

[24] Mosaberpanah, M.; Umar, S., Utilizing Rice Husk Ash as Supplement to Cementitious Materials on Performance of Ultra High Performance Concrete: -A review. *Mater. Today Sustain.*, **2020**, *7-8*, 100030, https://doi.org/10.1016/j.mtsust.2019.100030.

[25] Khoshnood, M. E.; Sharifian, S.; Asasian-Kolur, N., Alkaline activating agents for activation of rice husk biochar and simultaneous bio-silica extraction. *Bioresour. Technol. Rep.*, **2021**, *16*, 100853, https://doi.org/10.1016/j.biteb.2021.100853.

[26] Wang, L.; Zhao, M.; Ma, H.; Han, G.; Yang, D.; Chen, D.; Zhang, Y.; Zhou, J., Extraction of SiO_2 from gasified rice husk carbon simultaneously rice husk activated carbon production: Restudy on product properties, activation mechanism, and evolution law of pore structure. *Energy Rep.*, **2020**, *6*, 3094-3103, https://doi.org/10.1016/j.egyr.2020.11.031.

[27] Mohammed, Z.; Jeelani, S.; Rangari, V., Low temperature plasma treatment of rice husk derived hybrid silica/carbon biochar using different gas sources. *Mater. Lett.*, **2021**, *292*, 129678, https://doi.org/10.1016/j.matlet.2021.129678.

[28] Song, J.; Guo, S.; Ren, D.; Liu, H.; Kou, L.; Su, J.; Zheng, P., Rice husk-derived SiOx@carbon nanocomposites as a high-performance bifunctional electrode for rechargeable batteries. *Ceram. Int.*, **2020**, *46*, 11570-11576, https://doi.org/10.1016/j.ceramint.2020.01.185.

[29] Hou, J.; Mao, X.; Wang, J.; Liang, C.; Liang, J., Preparation of rice husk-derived porous hard carbon: A self-template method for biomass anode material used for high-performance lithium-ion battery. *Chem. Phys.*, **2021**, *551*, 111352, https://doi.org/10.1016/j.chemphys.2021.111352.

[30] Sudarman, S.; Andriayani, T.; Taufik, M., Synthesis and application of nano-silicon prepared from rice husk with the hydrothermal method and its use for anode lithium-ion batteries. *Mater. Sci. Energy Technol.*, **2024**, *7*, 1-8, https://doi.org/10.1016/j.mset.2023.07.003.

[31] Feng, Y.; Jiang, J.; Xu, Y.; Wang, S.; An, W.; Chai, Q.; Prova, U. H.; Wang, C.; Huang, G., Biomass derived diverse carbon nanostructure for electrocatalysis, energy conversion and storage. *Carbon*, **2023**, *211*, 118105, https://doi.org/10.1016/j.carbon.2023.118105.

[32] Jin, C.; Nai, J.; Sheng, O.; Yuan, H.; Zhang, W.; Tao, X.; Lou, X. W. D., Biomass-based materials for green lithium secondary batteries. *Energy Environ. Sci.*, **2021**, *14*, 1326-1379, https://doi.org/10.1039/d0ee02848g.

[33] Li, Q.; Liu, Y.; Wang, Y.; Chen, Y.; Guo, X.; Wu, Z.; Zhong, B., Review of the application of biomass-derived porous carbon in lithium-sulfur batteries. *Ionics*, **2020**, *26*, 4765-4781, https://doi.org/10.1007/s11581-020-03694-3.

[34] Wazir, A. H.; Wazir, I. U.; Wazir, A. M., Preparation and characterization of rice husk based physical activated carbon. *Energy Sources Part A: Recovery, Utilization, and Environmental Effects*, **2020**, 1-11. https://doi.org/10.1080/15567036.2020.1715512.

[35] Raut, E. R.; Bedmohata, M. A.; Chaudhari, A. R., Comparative study of preparation and characterization of activated carbon obtained from sugarcane bagasse and rice husk by using H_3PO_4 and $ZnCl_2$. *Mater. Today Proc.*, **2022**, 66, 1875-1884, https://doi.org/10.1016/j.matpr.2022.05.413.

[36] Alam, M. M.; Hossain, M. A.; Hossain, M. D.; Johir, M.; Hossen, J.; Rahman, M. S.; Zhou, J. L.; Hasan, A.

K.; Karmakar, A. K.; Ahmed, M. B., The Potentiality of Rice Husk-Derived Activated Carbon: From Synthesis to Application. *Processes,* **2020**, *8*, 203. https://doi.org/10.3390/pr8020203.

[37] Chen, J.; Liu, J.; Wu, D.; Bai, X.; Lin, Y.; Wu, T.; Zhang, C.; Chen D.; Li, H., Improving the supercapacitor performance of activated carbon materials derived from pretreated rice husk. *J. Energy Storage*, **2021**, *44*, 103432, https://doi.org/10.1016/j.est.2021.103432.

[38] Cui, J.; Cheng, F.; Lin, J.; Yang, J.; Jiang, K.; Wen, Z.; Sun, J., High surface area C/SiO_2 composites from rice husks as a high-performance anode for lithium ion batteries. *Powder Technol.*, **2017**, *311*, 1-8. https://doi.org/10.1016/j.powtec.2017.01.083.

[39] Liu, X. Y.; Huang, M.; Ma, H. L.; Zhang, Z. Q.; Gao, J. M.; Zhu, Y. L.; Han, X. J.; Guo, X. Y., Preparation of a Carbon-Based Solid Acid Catalyst by Sulfonating Activated Carbon in a Chemical Reduction Process. *Molecules*, **2010**, *15*, 7188-7196, https://doi.org/10.3390/molecules15107188.

[40] Lims, S. C.; Divya, S.; Manivannan, M.; Arumanayagam, T.; Robert, R.; Jose, M., Investigation of structural, temperature and frequency dependent dielectric behavior of Zn_2SnO_4@amorphous SiO_2 core shell nanocomposites. *Chem. Phys. Impact*, **2024**, *8*, 100485. https://doi.org/10.1016/j.chphi.2024.100485

[41] Hayashi, J.; Kazehaya, A.; Muroyama, K.; Watkinson, A., Preparation of activated carbon from lignin by chemical activation. *Carbon*, **2000**, *38*, 1873-1878, https://doi.org/10.1016/s0008-6223(00)00027-0.

[42] Dolgov, A.; Lopaev, D.; Lee, C.; Zoethout, E.; Medvedev, V.; Yakushev, O.; Bijkerk, F., Characterization of carbon contamination under ion and hot atom bombardment in a tin-plasma extreme ultraviolet light source. *Appl. Surf. Sci.*, **2015**, *353*, 708-713, https://doi.org/10.1016/j.apsusc.2015.06.079.

[43] Yang, S. Y.; Liu, L.; Jia, Z. X.; Fu, W. W.; Jia, D. M.; Luo, Y. F., Study on the structure-properties relationship of natural rubber/SiO_2 composites modified by a novel multi-functional rubber agent. *Express Polym. Lett.*, **2014**, *8*, 425-435, https://doi.org/10.3144/expresspolymlett.2014.46.

[44] Zhong, Y.; Qiu, X.; Gao, J.; Guo, Z., Chemical Structure of Si–O in Silica Fume from Ferrosilicon Production and Its Reactivity in Alkali Dissolution. *ISIJ International*, **2019**, *59*, 1098-1104, https://doi.org/10.2355/isijinternational.isijint-2018-516.

[45] Li, H. F.; Dimitrijev, S.; Sweatman, D.; Harrison, H. B.; Tanner, P.; Feil, B., Investigation of nitric oxide and Ar annealed SiO_2/SiC interfaces by x-ray photoelectron spectroscopy. *J. Appl. Phys.*, **1999**, *86*, 4316-4321, https://doi.org/10.1063/1.371363.

[46] Kim, N.; Lee, W.; Kim, J.; Kim, D.; Jang, B., Synthesis of passively prelithiated SiOx nanoparticles for Li-ion battery anode. *J. Am. Ceram. Soc.*, **2023**, *106*, 4554-4566, https://doi.org/10.1111/jace.19102.

[47] Li, Y.; Qian, Y.; Zhou, J.; Lin, N.; Qian, Y., Molten-LiCl induced thermochemical prelithiation of SiOx: Regulating the active Si/O ratio for high initial Coulombic efficiency. *Nano Res.*, **2021**, *15*, 230-237. https://doi.org/10.1007/s12274-021-3464-2.

[48] Ashuri, M.; He, Q.; Shaw, L. L., Silicon oxides for Li-ion battery anode applications: Toward long-term cycling stability. *J. Power Sources*, **2023**, *559*, 232660, https://doi.org/10.1016/j.jpowsour.2023.232660.

[49] Feng, Y.; Liu, X.; Liu, L.; Zhang, Z.; Teng, Y.; Yu, D.; Sui, J.; Wang, X., SiO_2/C Composite Derived from Rice Husks with Enhanced Capacity as Anodes for Lithium-Ion Batteries. *Chem. Select*, **2018**, *3*, 10338-10344, https://doi.org/10.1002/slct.201802353.

[50] Duong, M. V.; Nguyen, H. V.; Garg, A.; Tran, M. V.; Le, P. M. L., Strategy for Long Cycling Performance of Graphite/$LiNi_{1/3}Mn_{1/3}Co_{1/3}O_2$ Full-Cell Through High-Efficiency Slurry Preparation. *J. Electrochem. Soc.*, **2020**, *167*, 160533, https://doi.org/10.1149/1945-7111/abd1f6.

[51] Luo, M. F.; Rodrigues, M. T.; Shaw, L. L.; Abraham, D. P., Examining Effects of Negative to Positive Capacity Ratio in Three-Electrode Lithium-Ion Cells with Layered Oxide Cathode and Si Anode. *ACS Appl. Energy Mater.*, **2022**, *5*, 5513-5518,

https://doi.org/10.1021/acsaem.2c00665.

[52] Wu, W.; Kang, Y.; Wang, M.; Xu, D.; Wang, J.; Cao, Y.; Wang, C.; Deng, Y., An ultrahigh-areal-capacity SiOx negative electrode for lithium ion batteries. *J. Power Sources*, **2020**, *464*, 228244. https://doi.org/10.1016/j.jpowsour.2020.228244.

[53] Abe, Y.; Kumagai, S., Effect of negative/positive capacity ratio on the rate and cycling performances of $LiFePO_4$/graphite lithium-ion batteries. *J. Energy Storage*, **2018**, *19*, 96-102, https://doi.org/10.1016/j.est.2018.07.012.

[54] Dörfler, S.; Althues, H.; Härtel, P.; Abendroth, T.; Schumm, B.; Kaskel, S., Challenges and Key Parameters of Lithium-Sulfur Batteries on Pouch Cell Level. *Joule*, **2020**, *4*, 539-554, https://doi.org/10.1016/j.joule.2020.02.006.